Journal of Power Sources 195 (2010) 3977–3983

Contents lists available at ScienceDirect

Journal of Power Sources

journal homepage: www.elsevier.com/locate/jpowsour

Platinum/tin oxide/carbon cathode catalyst for high temperature PEM fuel cell

Javier Parrondo[a], Federico Mijangos[b], B. Rambabu[a,*]

[a] Solid State Ionics and Surface Science Laboratory, Department of Physics, Southern University and A&M College, Baton Rouge, LA 70813, USA
[b] Department of Chemical Engineering, University of the Basque Country, Bilbao, Vizcaya 48940, Spain

ARTICLE INFO

Article history:
Received 10 December 2009
Received in revised form 12 January 2010
Accepted 13 January 2010
Available online 21 January 2010

Keywords:
High temperature PEMFC
PBI (polybenzimidazole)
Platinum
Tin oxide
Durability

ABSTRACT

The performance of high temperature polymer electrolyte fuel cell (HT-PEMFC) using platinum supported over tin oxide and Vulcan carbon (Pt/SnOx/C) as cathode catalyst was evaluated at 160–200 °C and compared with Pt/C. This paper reports first time the Pt/SnOx/C preparation, fuel cell performance, and durability test up to 200 h. Pt/SnOx/C of varying SnO compositions were characterized using XRD, SEM, TEM, EDX and EIS. The face-centered cubic structure of nanosized Pt becomes evident from XRD data. TEM and EDX measurements established that the average size of the Pt nanoparticles were ~6 nm. Low ionic resistances were derived from EIS, which ranged from 0.5 to 5 Ω-cm^2 for cathode and 0.05 to 0.1 Ω-cm^2 for phosphoric acid, doped PBI membrane. The addition of the SnOx to Pt/C significantly promoted the catalytic activity for the oxygen reduction reaction (ORR). The 7 wt.% SnO in Pt/SnO_2/C catalyst showed the highest electro-oxidation activity for ORR. High temperature PEMFC measurements performed at 180 °C under dry gases (H_2 and O_2) showed 0.58 V at a current density of 200 mA cm^{-2}, while only 0.40 V was obtained in the case of Pt/C catalyst. When the catalyst contained higher concentrations of tin oxide, the performance decreased as a result of mass transport limitations within the electrode. Durability tests showed that Pt/SnOx/C catalysts prepared in this work were stable under fuel cell working conditions, during 200 h at 180 °C demonstrate as potential cathode catalyst for HT-PEMFCs.

1. Introduction

The high temperature polymer electrolyte membrane fuel cells (HT-PEMFCs) technology is particularly attractive for transportation application, because they do not use the conventional Nafion® based membranes and are exceptionally clean, producing none of the harmful emissions generally associated with combustion engines. However, the success of the fuel cell commercialization must entail the use of less expensive materials both in the electrolyte membrane and in the cathode catalyst. Platinum based catalysts are recognized as the best electrocatalysts for use in PEMFCs and phosphoric acid fuel cells. So far, fuel cells have only marginal applications and are by large confined to demonstration purposes due to the increased use of expensive Pt, and Nafion® based electrolytes. In recent years, several fuel cell research groups are focusing on developing cheaper catalysts to reduce the Pt content.

The slow oxygen reduction reaction (ORR) kinetics on Pt catalysts is among the most limiting factors in the energy conversion efficiency of the state-of-the-art PEMFC. To increase the activity towards ORR some non-noble metal catalysts such as Cu and Ni, transition metal N4-macrocycles such as porphyrin complexes, and metal oxides have been investigated as possible cathode catalysts for fuel cells [1–8]. However, some of these catalysts suffered the oxidation and dissolution due to the presence of phosphoric acid at high temperatures. The higher ORR activity was found on anodically formed TiO_2 on Ti surface. The reaction proceeds through a two-electron process in acidic medium and four-electron process in basic solutions [9]. Perovskite type compounds, like lanthanum manganite, have also been proposed as catalysts for ORR. They showed good cathodic performance above −0.15 V under ambient temperatures [10]. The main disadvantage, when using these oxides, is the low electronic conductivity leading to large ohmic losses in the electrodes, although, significant progress has been made in the development of oxide modified Pt electrocatalysts for PEMFC that show enhanced electrochemical activity [11–18]. The results show that metal oxide-promoted Pt catalysts (PtWO_3/C, PtMnO_2/C, PtCrO_2/C, PtV_2O_5/C) are more active than pure Pt catalysts [19–22].

Very recently, nanoparticle metal supported over tin oxide with different Pt/Sn ratios were prepared by polyol method at 80 °C. The electrochemical activity and selectivity of these catalysts for ethanol electro-oxidation increased with tin content [23]. Gold nanoparticles supported on hydrous tin oxide (Au/SnOx) showed improved activity for the ORR through a four-electron oxygen reduction reaction in an acid electrolyte, in contrast with the 2–3 electron ORR commonly observed with traditional Au catalysts.

* Corresponding author. Tel.: +1 225 771 2493; fax: +1 225 771 2310.
E-mail address: rambabu@cox.net (B. Rambabu).

0378-7753/$ – see front matter © 2010 Elsevier B.V. All rights reserved.
doi:10.1016/j.jpowsour.2010.01.027

The unique electrocatalytic activity of the Au–SnO is confirmed by the low amount of peroxide detected and the high electrocatalytic activity of the Au–SnO is attributed to metal support interactions [24].

Unlike the previous reports on Pt/SnO, this work focuses on the preparation and characterization of Pt/SnOx/C, with varying SnO compositions, as cathode catalyst for PBI-based HT-PEMFC. Fuel cell performance measurements, in the temperature regime 160–200 °C, and durability test up to 200 h were done in order to determine their stability and feasibility as cathode catalyst for HT-PEMFCs.

2. Material and methods

2.1. Materials

Lithium chloride (99%), citric acid (98%), 3,3′-diaminobenzidine (99%), *N*,*N*′-dimethylacetamide (99.5%), XC72R carbon powder and polyphosphoric acid (115%) were purchased from Sigma–Aldrich. Hexachloroplatinic acid (99.9%), isophthalic acid (99%), sodium borohydride (98%), tin(II) chloride (99%) and platinum, nominally 40 wt.% on carbon black were purchased from Alfa Aesar.

2.2. Fabrication of catalyst support

SnOx/C with SnO loadings ranging from 10 to 40% by weight (wt.%) were prepared following a modification of the procedure described by Baker et al. [24]. In a typical synthesis, 1 g of Vulcan carbon and the required amount of $SnCl_2$ were added to 150 mL distilled water and stirred for 30 min. Tin oxide was formed upon precipitation of Sn^{2+} using 20 mL 1 M ammonium hydroxide (added dropwise). The resulting suspension was stirred for 2 h, filtered, and then washed copiously with de-ionized water to remove unreacted materials. Afterwards it was dried under vacuum at room temperature, and placed in an oven at 150 °C to get the final product. The resulting material is a non-stoichiometric oxide (SnOx), but we are giving the composition of the materials assuming the reduced state (SnO).

2.3. Fabrication of Pt supported over SnOx/C

Aqueous solution of hexachloroplatinic acid (100 mL) was mixed with citric acid and stirred for 30 min to form complexes. To the yellow colored solution, 0.3 g of SnO/C support was added and stirred for 1 h. 0.3 g of $NaBH_4$ dissolved in 50 mL de-ionized water (freshly prepared) was added dropwise to the above suspension and stirred continuously for 2 h. Finally, the suspension was filtered, washed copiously with de-ionized water and dried under vacuum at room temperature overnight. SnO/C supported Pt nanoparticles with 7, 12, 18 and 24 wt.% SnO were prepared. The nominal Pt loading was 40 wt.% in all the catalysts.

2.4. Characterization of the catalyst

The prepared materials were characterized by X-ray diffraction (XRD), scanning electron microscopy (SEM), and transmission electron microscopy (TEM) for the phase identification and morphology, respectively. XRD measurements were performed on a Rigaku D/max-RA X-ray diffractometer using a CuKα source ($\lambda = 1.5406$ Å) operated at 40 kV and a scan rate of $0.04^\circ\ s^{-1}$ over the 2θ range of 10–90°. A Phillips CM200 microscope equipped with a LaB_6 filament and a super twin lens operating at 200 kV was used to record TEM images. Scanning electron microscope, JEOL JSM-7000F, with field emission cathode operating at 20 kV was used in the characterization. The system was equipped with an EDX detector.

2.5. Synthesis of m-polybenzimidazole and membrane preparation

m-PBI was synthesized following the procedure described by Xiao et al. [25]. In a typical synthesis, 3.7135 g of isophthalic acid (22.35 mmol) and 4.7896 g of 3,3′-diaminobenzidine (22.35 mmol) were added to a three-neck reaction flask in an Argon filled glovebox, followed by 91.5 g of polyphosphoric acid. The reaction mixture was stirred using a mechanical overhead stirrer and purged with a slow stream of nitrogen and maintained at 190–220 °C for 16–24 h. Inherent viscosity (IV) of the polymer was measured at a polymer concentration of $2\ kg\ m^{-3}$ in concentrated sulfuric acid (96 wt.%) at room temperature using an Ubbelohde viscometer.

The membranes used in the fabrication of MEAs were prepared by casting the polyphosphoric acid (PPA) polymer solution onto glass plates using an adjustable film applicator (GARDCO MICROM II, Paul N. Gardner Company). The gate clearance was fixed in 0.015 cm to obtain membranes of approximately 100 μm after hydrolysis. Since PPA is extremely hygroscopic, moisture is absorbed from the atmosphere and PPA is hydrolyzed to phosphoric acid producing a gel membrane [26]. The concentration of phosphoric acid was estimated by weighing a membrane sample before and after removing phosphoric acid by washing with ammonium hydroxide.

2.6. Membrane electrode assembly (MEA) fabrication and high temperature PEMFC testing

MEAs with an active area of 3.24 cm^2 were assembled by placing two gas diffusion electrodes (GDEs) on both sides of the PBI membrane. The MEA was assembled in a 5 cm^2 single cell PEMFC with single serpentine flow fields (Fuel Cell Technologies, Inc.), using sub-gaskets to avoid direct pressure of the gaskets over the membrane and hence protecting the membrane from excessive pressure and stress during heating. The sub-gaskets had a thickness of 25 μm and the gaskets 395 μm. The pinch, defined as the difference between thickness of the MEA and the gaskets, was 75 μm.

PBI solution (5 wt.%) in *N*,*N*′-dimethylacetamide was prepared with the aid of lithium chloride (1.5 wt.%) in an autoclave at 250 °C and 6.3 bar for 6 h. The homogeneous solution obtained was subsequently used to prepare catalyst ink [27]. Gas diffusion electrodes

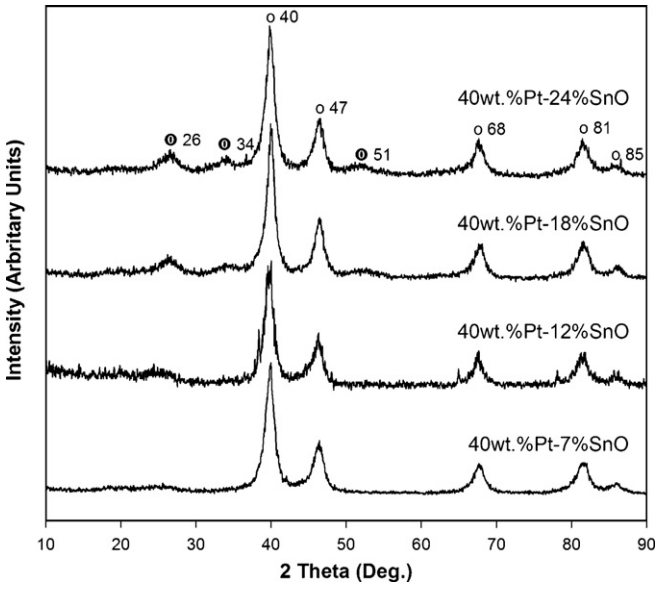

Fig. 1. XRD of Pt/SnOx/C catalyst.

were prepared by painting over the microporous area of a gas diffusion layer (GDL Sigracet GDL 10BB, 420 μm, SGL Carbon Group) with an airbrush. Catalyst ink consisted of home-made catalyst (0.2 g) to which DMAc (7.5 g) and 5 wt.% PBI solution (0.211 g) were added. The ink slurry was stirred overnight to break up the catalyst powder in order to get a homogenous ink. During painting, the gas diffusion layer was kept near an IR lamp to dry the ink between each application. The metal loading of each electrode was measured by the difference in weight before and after painting and was kept in $0.50 \pm 0.05\ mg\ cm^{-2}$. The anode was fabricated using commercial Pt/C catalyst (platinum nominally 40% on carbon black, Alfa Aesar) with a loading of $0.5\ mg\ Pt\ cm^{-2}$.

The performance was evaluated after conditioning the MEAs during 24 h at $200\ mA\ cm^{-2}$ and 160 °C to keep steady state conditions. The measurements were made by using a Compact Fuel Cell Test System model 850e (Scribner Associates, Inc.) controlled using FuelCell® 3.9c software. The polarization curves were recorded at atmospheric pressure using dry oxygen and hydrogen at temperatures ranging from 160 to 200 °C. Stoichiometric flows (1.2 stoichiometric ratio for hydrogen and 2 for oxygen) were employed. Minimum flows were $0.1\ L\ min^{-1}$ at the anode and $0.2\ L\ min^{-1}$ at the cathode. Cell resistance was measured by using current-interrupt technique.

Cyclic voltammetry (CV) and linear sweep voltammetry (LSV) were used to check the amount of active catalyst, the crossover of reactants and the absence of short-circuits. The tests were performed using $0.2\ L\ min^{-1}$ of dry hydrogen at the anode side (reference and counter electrode) and $0.2\ L\ min^{-1}$ of dry nitrogen at the cathode side (working electrode). CV was recorded in the potential range of 0.05–0.8 V at a scan rate of $40\ mV\ s^{-1}$ and LSV in the potential range of 0.15–0.5 V at a scan rate of $2\ mV\ s^{-1}$. The coulombic charge for hydrogen desorption (Q_H) was used to calculate the ECA of the electrodes [28]. Only cells demonstrating low hydrogen crossover and no shorting were chosen for further testing.

AC impedance spectra were recorded using the built-in FRA of Fuel Cell Test System model 850e. The cathode and anode were working electrode and counter electrode, respectively. A galvanostatic AC signal of 10% DC was applied in the frequency range 5 kHz to 0.1 Hz. Impedance measurements were taken after stabilization of the system for at least 15 min.

3. Results and discussion

3.1. Characterization of the polymer

PBI polymer was characterized by means of inherent viscosity (IV) and phosphoric acid content. The acid content of the PBI membrane that was prepared in-house was 85 wt.%, in agreement with reported data. This weight is in correspondence to

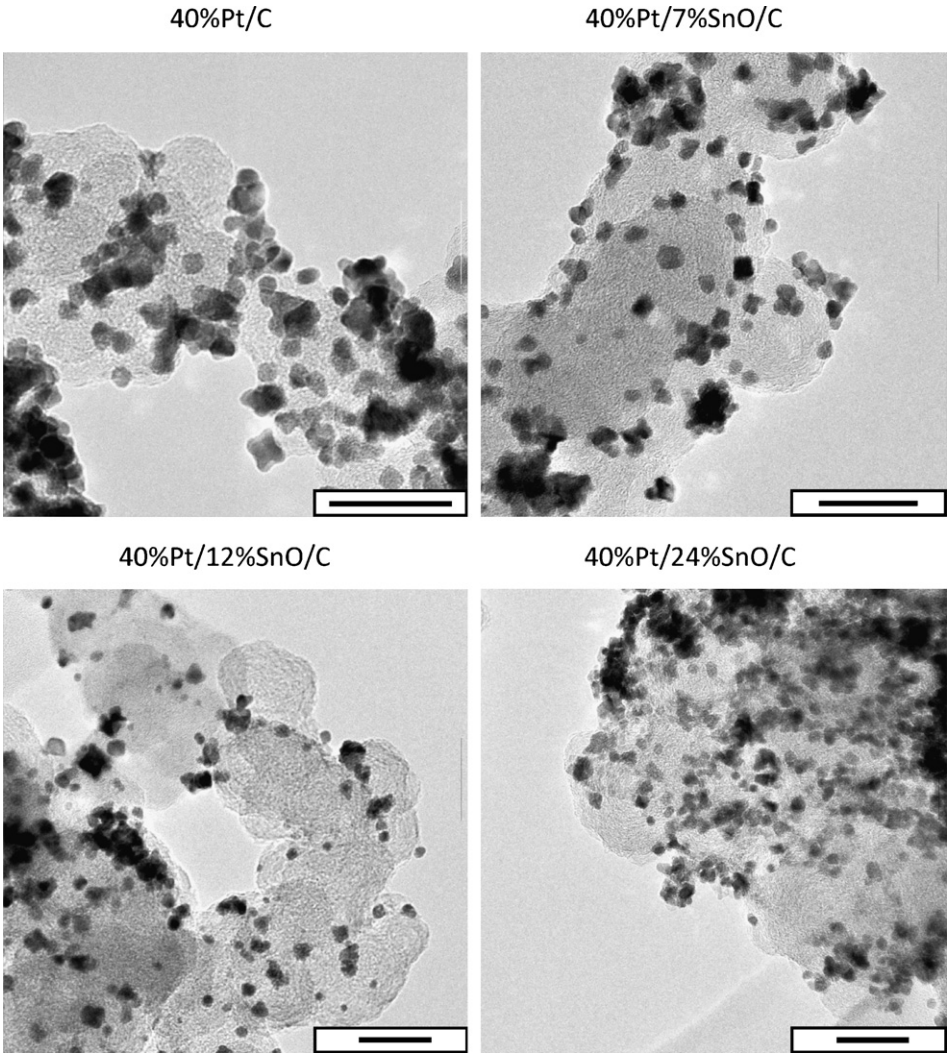

Fig. 2. TEM of Pt/SnOx/C catalyst (scale bar 30 nm).

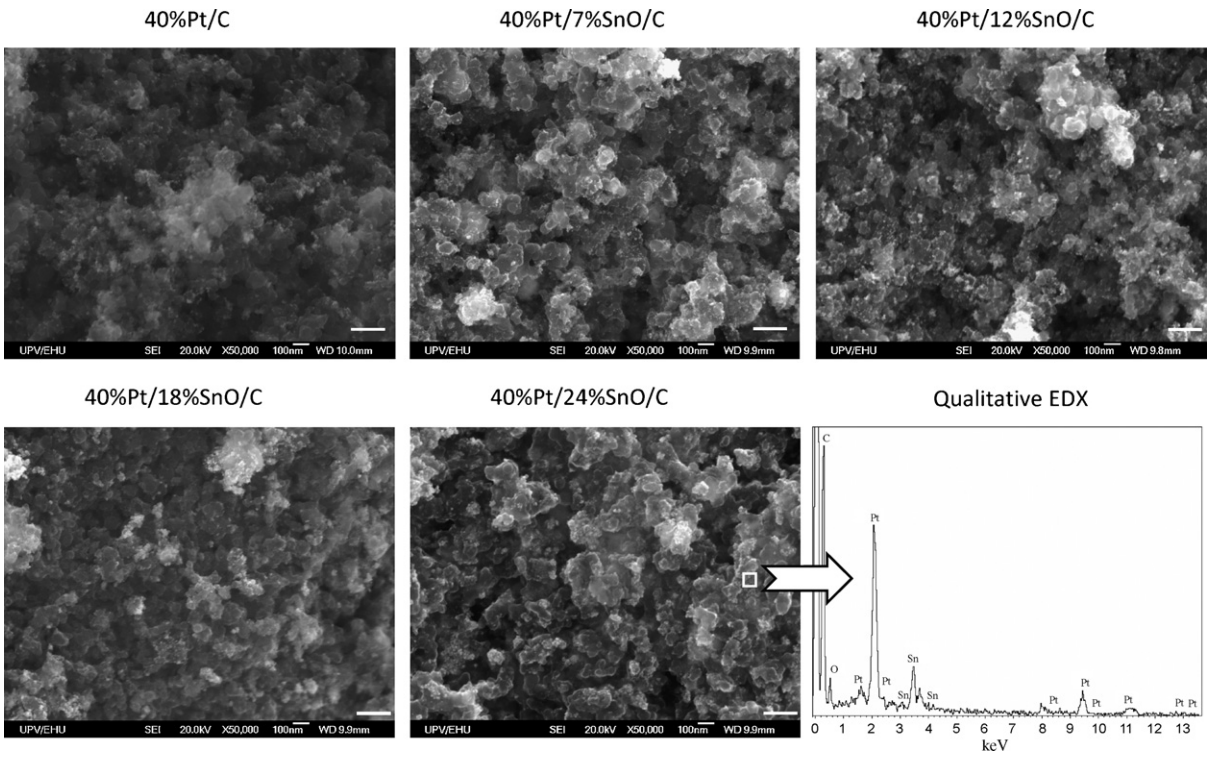

Fig. 3. SEM and EDX of Pt/SnOx/C catalyst (scale bar 200 nm).

18 mol of phosphoric acid per mol of polymer repeating unit, which yields the conductivities of 0.1 S cm^{-1} at 180 °C [29]. Inherent viscosity, which is an indirect measure of the molecular weight, was in the interval of 0.7–0.9 dL g^{-1}, depending on the batch, in agreement with published data [29,30]. The molecular weight calculated using Mark–Houwink expression was in the interval 115,000–150,000 g mol^{-1} which corresponds to moderate molecular weight polymer [30].

3.2. Characterization of the catalysts

XRD patterns of the Pt/SnOx/C catalysts are shown in Fig. 1. As expected, the catalysts have crystalline structure with peaks at 2θ values of 40°, 47°, 68°, 81° and 85°, corresponding to the (1 1 1), (2 0 0), (2 2 0), (3 1 1) and (2 2 2) planes of face-centered cubic (fcc) structure of Pt (JCPDS No. 87-0640), respectively. The average crystallite size of the platinum in these catalysts, obtained using the Debye–Scherrer formula from the broadening of the (2 2 0) diffraction peak (Gaussian–Lorentzian peak) according to Scherrer's equation [31], was estimated to be approximately 6.0 ± 0.5 nm. This value was in agreement with the nanoparticle diameter estimated from TEM images (Fig. 2). The positions of the Pt diffraction peaks remained constant in the Pt/SnOx/C catalysts, indicating that these materials are composed only of Pt without any alloy phase formation. This point was confirmed by EDX analysis of Pt particles. There were other minor peaks at 2θ values of 26°, 34° and 51° and the height of these peaks increased with an increase in the amount of SnO (PCPDF 411445). Like Pt peaks, these peaks are also broad confirming that SnO is also finely distributed within the carbon support.

The TEM photographs of Pt/SnOx/C electrocatalysts are shown in Fig. 2, showing the morphology and dispersion of Pt over the SnOx/C support. In these pictures, the semitransparent clusters are the aggregates of carbon black particles and tin oxide, and the black nanoparticles are the dispersed platinum particles. The presence of SnO in the catalyst cannot be observed in TEM images and there is no change in the morphology of the samples when the concentration of tin oxide is increased. Complimentary information about sample morphology can be found by examining the SEM images in Fig. 3. Brighter areas in the images correspond to Pt and SnO nanoparticles that seem to be well distributed over the support as expected by the preparation method. The larger particles of the support are around 100 nm and no apparent differences in the morphology are observed depending on the SnOx content. The EDX spectrum shown also in Fig. 3 confirms the presence of Pt and Sn in the Pt/SnOx/C catalysts.

3.3. Electrochemically active areas (ECA) and crossover currents

As can be seen in Table 1, ECA for the Pt/SnOx/C MEAs were below 5 m^2 g^{-1} Pt at 180 °C. Although these values are lower than those of Nafion®-based MEAs at 80 °C (30–40 m^2 g^{-1} Pt), they are

Table 1
Electrochemically active areas (ECA), open circuit voltages (OCV), and crossover currents of Pt/SnOx/C based MEAs at 180 °C.

SnO conc. (wt.%)	OCV (V)	ECA (m^2 g^{-1} Pt)	Crossover current (mA cm^{-2})	Presence of short-circuit
0	0.95	3.7	1.8	No
7	0.85	4.9	2.7	No
12	0.85	5.0	2.8	No
18	0.93	2.0	0.3	No
24	0.77	4.3	2.6	No

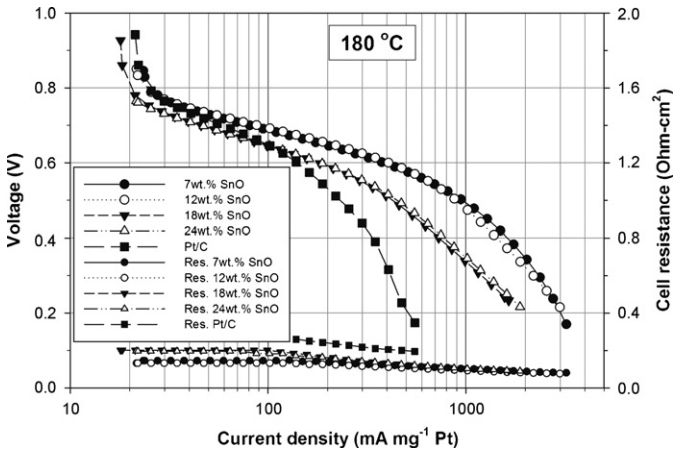

Fig. 4. Polarization curves of PBI-based MEAs at 180 °C using of Pt/SnOx/C catalyst at the cathode. H_2 (dry) stoichiometric ratio: 1.2; O_2 (dry) stoichiometric ratio: 2; minimum flow at the anode: 0.1 L min^{-1}; minimum flow at the cathode: 0.2 L min^{-1}; pressure: 1 atm; Pt loading (anode and cathode): 0.5 mg cm^{-2}.

still reasonable for PBI-based MEAs [32–34]. Open circuit voltages are in the range of 0.8–0.99 V. They are lower in the case of materials having higher percentages of SnO. This is due to the mixed potentials in the electrode produced as a consequence of the oxidation of electrode materials: SnO, carbon, and impurities. Hydrogen crossover currents are below 3 mA cm^{-2} and linear sweep voltammetry does not reveal the presence of any short-circuit in the MEAs.

3.4. Performance of Pt/SnO/C based MEAs

The fuel cell performance curves recorded at 180 °C for the MEAs prepared using Pt/SnO/C catalyst in the cathode are shown in Fig. 4. The measurements indicate that best performance is obtained with MEAs prepared using catalysts with 7 wt.% SnO. Potentials around 0.65 V were observed at currents of 0.2 A mg^{-1} Pt.

Impedance spectra (IS), recorded using oxygen as oxidant in the region of activation loss (0.1 A) was employed in order to get information on mass transfer in the vicinity of the catalyst active surface. The spectra recorded under these conditions is shown in Fig. 5a and holds constant for all the catalysts, probing that mass transfer in the vicinity of the active surface was similar in all the catalysts. With higher concentrations of tin oxide the performance decreased due to mass transport limitations, as can be seen in Fig. 5b, by the increase of the diameter of the arc in Nyquist plot from 0.3 Ω-cm^2 for 7 wt.% SnO to 0.9 Ω-cm^2 in the case of 24 wt.% SnO catalyst. Increased mass-transfer resistance is due to the decrease of active surface area of the support as a result of precipitation of tin oxide. The catalyst active surface becomes less accessible due to the increase of diffusion paths and mass-transfer resistance.

The ohmic resistance of the cathode increases when the concentration of tin oxide was raised from 7 to 18 wt.% (see Table 2), but decreases slightly when it was increased to 24 wt.% SnO (probably because of changes in the dispersion of SnOx within the support).

Table 2
Effect of the concentration of SnO on ionic resistance at different temperatures.

SnO conc. (%)	Re @160 °C (Ω-cm^2)	Re @180 °C (Ω-cm^2)	Re @200 °C (Ω-cm^2)
7	0.3	0.7	1.0
12	1.8	0.9	2.3
18	2.0	3.2	4.6
24	–	1.9	2.7

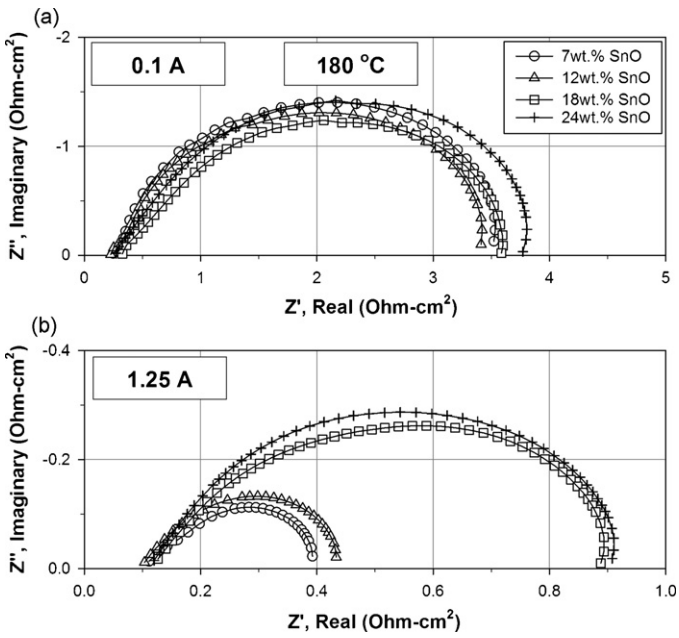

Fig. 5. Nyquist plots showing the effect of the concentration of SnO on (a) electrochemical reaction resistance and (b) cathode mass-transfer resistances. Temperature 180 °C. H_2 stoichiometric ratio: 1.2; O_2 stoichiometric ratio: 2; minimum flow at the anode: 0.1 L min^{-1}; minimum flow at the cathode: 0.2 L min^{-1}; pressure: 1 atm; Pt loading (anode and cathode): 0.5 mg cm^{-2}.

3.5. Effect of temperature on the performance of 7 wt.% SnO MEAs

The effect of temperature on the performance of 7 wt.% SnO based MEAs is shown in Fig. 6. Best results were obtained when the MEAs were operated in the interval 160–180 °C. At 200 mA cm^{-2} and an operating temperature of 180 °C using dry hydrogen and oxygen at atmospheric pressure, a voltage of 0.58 V was produced. With similar Pt loadings and using in-house Pt/C catalysts under same operating conditions, only 0.40 V were obtained. Membrane resistances for 7 wt.% SnO MEAs were in the range 0.1–0.15 Ω-cm^2 (Fig. 6) depending on operating current density. At high currents the resistance was slightly lower probably due to the production of more water that hydrates the membrane thus enhancing the transport of protons.

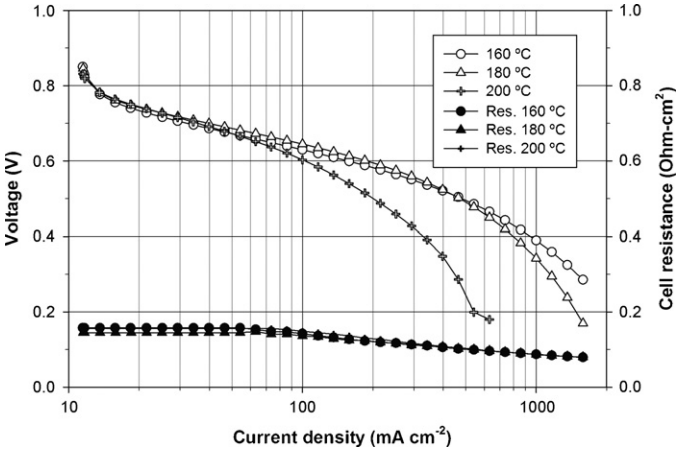

Fig. 6. Polarization curves of PBI-based MEAs manufactured using 40 wt.%Pt/7%SnO/53%C catalyst. H_2 (dry) stoichiometric ratio: 1.2; O_2 (dry) stoichiometric ratio: 2; minimum flow at the anode: 0.1 L min^{-1}; minimum flow at the cathode: 0.2 L min^{-1}; pressure: 1 atm; Pt loading (anode and cathode): 0.5 mg cm^{-2}.

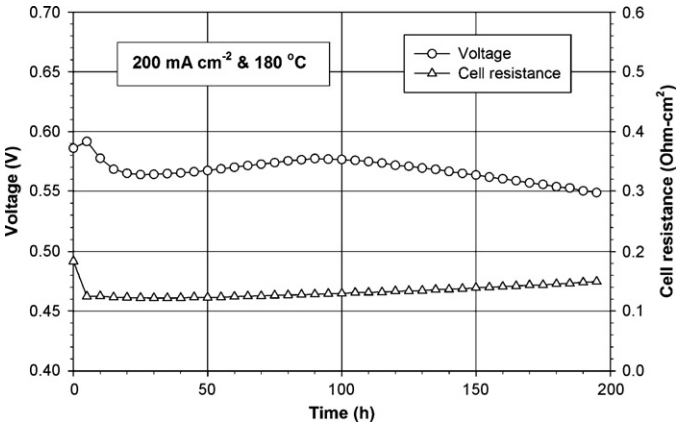

Fig. 7. Durability of MEA prepared using 40 wt.%Pt/7%SnO/53%C catalyst. H_2 (dry) stoichiometric ratio: 1.2; O_2 (dry) stoichiometric ratio: 2; minimum flow at the anode: 0.1 L min^{-1}; minimum flow at the cathode: 0.2 L min^{-1}; pressure: 1 atm; Pt loading (anode and cathode): 0.5 mg cm^{-2}.

3.6. Durability of Pt/SnOx–C catalysts

To confirm the stability of the catalyst under fuel cell working conditions, the MEA prepared with Pt/SnOx/C catalyst was run at 180 °C, during a 200 h time interval at a current density of 200 mA cm^{-2}. Polarization data and impedance spectra were also collected before and after running the experiment. The evolution of voltage and cell resistance during the durability experiment can be observed in Fig. 7. The voltage remained around 0.55 V with fluctuations of 20–25 mV during the experiment. The membrane resistance increased by 20% most likely due to the loss of phosphoric acid by evaporation or movement into the electrodes; this increase of the membrane resistance only increases the ohmic polarization by 5 mV.

As seen in Fig. 8, the OCV has been increased from 0.85 to 0.99 V after the experiment is completed. This is probably due to the less contribution of SnO to the mixed potential as a result of oxidation of the SnO to SnO_2. The performance of the MEA after the durability experiment is better in the activation region, but worse in the mass-transfer region (current densities greater than 100 mA cm^{-2}). The loss of the electrochemical performance at high current densities can be attributed to an increase of mass-transfer resistance as observed in Fig. 9b.

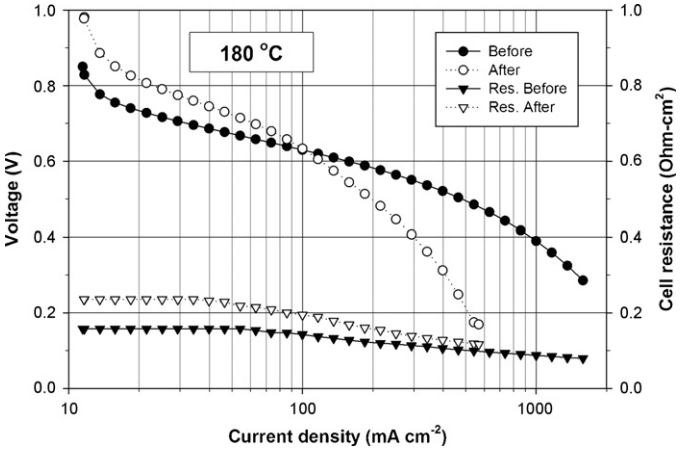

Fig. 8. Polarization curves of MEA prepared using 40 wt.%Pt/7%SnO/53%C catalyst, before and after durability experiment for 200 h. H_2 (dry) stoichiometric ratio: 1.2; O_2 (dry) stoichiometric ratio: 2; minimum flow at the anode: 0.1 L min^{-1}; minimum flow at the cathode: 0.2 L min^{-1}; pressure: 1 atm; Pt loading (anode and cathode): 0.5 mg cm^{-2}.

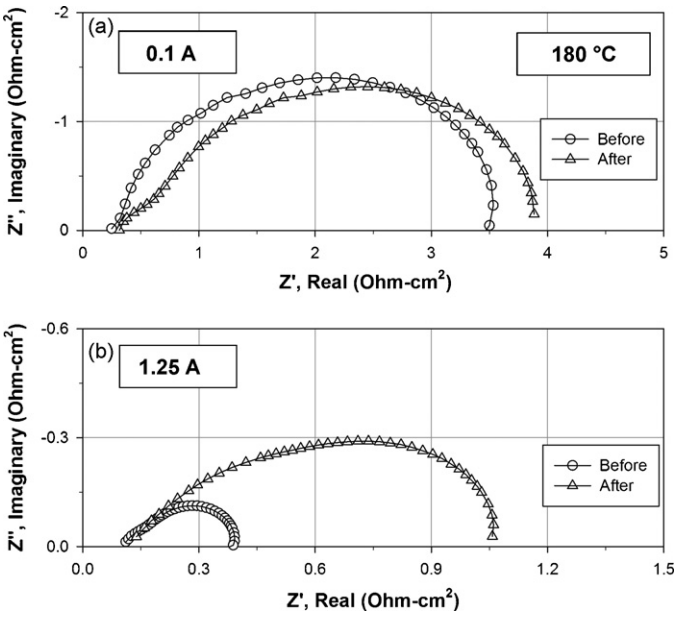

Fig. 9. Nyquist plots at 0.1 A (activation region) and 1.25 A (mass-transfer region) before and after durability experiment at 180 °C during 200 h. H_2 stoichiometric ratio: 1.2; O_2 stoichiometric ratio: 2; minimum flow at the anode: 0.1 L min^{-1}; minimum flow at the cathode: 0.2 L min^{-1}; pressure: 1 atm; Pt loading (anode and cathode): 0.5 mg cm^{-2}.

This increase in the mass-transfer resistance is probably due to the degradation of the support by the aggressive experimental conditions that lead to the oxidation of the carbon support. The decrease of the carbon active area and porosity increased the mass-transfer resistances through the electrodes. The loss of phosphoric acid is unlikely because at these temperatures, acid evaporation was found to be of no concern due to the unique properties of the sol–gel membrane produced through the polyphosphoric acid process [35]. Similarly the uptake of phosphoric acid (electrolyte) from the membrane seems unlikely because the electrode resistance increases after the experiment as can be seen by the increase of 45° branch observed at high frequencies in the Nyquist plot (Fig. 9a).

4. Conclusions

Pt/SnOx/C catalysts were prepared by wet chemistry procedures and characterized by XRD, SEM, TEM, EDX and electrochemical impedance spectroscopy (EIS). The average crystallite size of the platinum was estimated to be approximately 6.0 ± 0.5 nm. High temperature PEMFC measurements performed using PBI-based MEAs showed good performance when using catalysts containing 7 wt.% SnO in the cathode. 0.58 V was produced using this catalyst whereas 0.4 V were produced using in-house Pt/C catalyst at 200 mA cm^{-2}, 180 °C and using dry hydrogen and oxygen at atmospheric pressure. With higher concentrations of tin oxide the performance decreased as a result of mass transport limitations within the electrode, as confirmed by impedance spectroscopy measurements.

Durability tests performed during a 200 h time interval at 180 °C and 200 mA cm^{-2} showed that Pt/SnOx/C catalysts were stable under fuel cell working conditions. The good performance and durability of the Pt/SnOx/C catalysts make them good alternatives for cathodes for high temperature PEMFCs.

Acknowledgements

This work is supported by U.S-DOD-ARO under the grant # W911NF-08-C-0415. BRB and Javier Parrondo thank Dr. Robert

Mantz (Electrochemistry and Advanced Energy Conversion) at ARO-Chemical Sciences, and Dr. Thomas L. Reitz (Electrochemistry and Thermal Sciences at AFRL, Wright Patterson Airbase, OH) for supporting fuel cell research at SUBR.

References

[1] S. Ohno, K. Yagyuu, K. Nakatsuji, F. Komori, Surf. Sci. 554 (2004) 183–192.
[2] D. Kolovos-Vellianitis, Th. Kammler, J. Kuppers, Surf. Sci. 482–485 (2001) 166–170.
[3] D. Kolovos-Vellianitis, J. Kuppers, J. Phys. Chem. B 107 (2003) 2559–2564.
[4] B. Lescop, J.Ph. Jay, G. Fanjoux, Surf. Sci. 548 (2004) 83–94.
[5] A. Garsuch, K. MacIntyre, X. Michaud, D.A. Stevens, J.R. Dahn, J. Electrochem. Soc. 155 (2008) B953–B957.
[6] M. Tsuda, H. Kasai, Surf. Sci. 601 (2007) 5200–5206.
[7] J.H. Kim, A. Ishihara, S. Mitsushima, N. Kamiya, K.I. Ota, Chem. Lett. 36 (2007) 514–515.
[8] T.S. Olson, K. Chapman, P. Atanassov, J. Power Sources 183 (2008) 557–563.
[9] S.V. Mentus, Electrochim. Acta 50 (2004) 27–32.
[10] M. Hayashi, H. Uemura, K. Shimanoe, N. Miura, N. Yamazoe, J. Electrochem. Soc. 151 (2004) A158–A163.
[11] K. Drew, G. Girishkumar, K. Vinodgopal, P.V. Kamat, J. Phys. Chem. B 109 (2005) 11851–11857.
[12] K.W. Park, K.S. Ahn, Y.C. Nah, J.H. Choi, Y.E. Sung, J. Phys. Chem. B107 (2003) 4352–4355.
[13] P.K. Shen, A.C. Tseung, J. Electrochem. Soc. 141 (1994) 3082–3090.
[14] J.W. Guo, T.S. Zhao, J. Prabhuram, R. Chen, C.W. Wong, J. Power Sources 156 (2006) 345–354.
[15] C.L. Campos, C. Roldan, M. Aponte, Y. Ishikawa, C.R. Cabrera, J. Electroanal. Chem. 581 (2005) 206–215.
[16] K. Miyazaki, H. Ishihara, K. Matsuoka, Y. Iriyama, K. Kikuchi, Y. Uchimoto, T. Abe, Z. Ogumi, Electrochim. Acta 52 (2007) 3582–3587.
[17] M.B. Oliveira, L.P.R. Profeti, P. Olivi, Electrochem. Commun. 7 (2005) 703–709.
[18] Y. Bai, J. Wu, J. Xi, J. Wang, W. Zhu, L. Chen, X. Qiu, Electrochem. Commun. 7 (2005) 1087–1090.
[19] A. Trovarelli, F. Zamar, J. Llorca, C. De Leitenburg, G. Dolcetti, J.T. Kiss, J. Catal. 169 (1997) 490–502.
[20] A.C.C. Tseung, K.Y. Chen, Catal. Today 348 (1997) 439–441.
[21] K.Y. Chen, P.K. Shen, A.C.C. Tseung, J. Electrochem. Soc. 142 (1995) L185–L186.
[22] P.K. Shen, K.Y. Chen, A.C.C. Tesung, J. Electrochem. Soc. 142 (1995) L85–L86.
[23] H. Jiang, C. Yu, Z. Huang, H. Zhu, ECS Trans. 17 (1) (2008) 347–358.
[24] W.S. Baker, J.J. Pietron, M.E. Teliska, P.J. Bouwman, D.E. Ramaker, K.E. Swider-Lyons, J. Electrochem. Soc. 153 (2006) A1702–A1707.
[25] L. Xiao, H. Zhang, E. Scanlon, L.S. Ramanathan, E.W. Choe, D. Rogers, T. Apple, B.C. Benicewicz, Chem. Mater. 17 (2005) 5328–5333.
[26] J. Mader, L. Xiao, T.J. Schmidt, B.C. Benicewicz, Adv. Polym. Sci. 216 (2008) 63–124.
[27] J. Lobato, P. Canizares, M.A. Rodrigo, J.J. Linares, G. Manjavacas, J. Membr. Sci. 280 (2006) 351–362.
[28] A. Pozio, M. De Francesco, A. Cemmi, F. Cardellini, L. Giorgi, J. Power Sources 105 (2002) 13–19.
[29] T.J. Schmidt, J. Baurmeister, ECS Trans. 16 (2008) 263–270.
[30] E.W. Choe, US Patent US4312976 (1982).
[31] F. Miyaji, Y. Kono, Y. Suyama, Mater. Res. Bull. 40 (2005) 209.
[32] O.E. Kongstein, T. Berning, B. Børresen, F. Seland, R. Tunold, Energy 32 (2007) 418–422.
[33] J.C. Huang, W.E. O'Grady, E. Yeager, J. Electrochem. Soc. 124 (1977) 1732–1737.
[34] M.A. Habib, J.O'M. Bockris, J. Electrochem. Soc. 132 (1985) 108–114.
[35] T.J. Schmidt, ECS Trans. 1 (2006) 19–31.